The ^{17}O Hyperfine Interaction in $V^{17}O(H_2{}^{17}O)_5{}^{2+}$ and $Mn(H_2{}^{17}O)_6{}^{2+}$ Determined by High Field ENDOR Aided by DFT Calculations

Debbie Baute and Daniella Goldfarb*

Department of Chemical Physics, The Weizmann Institute of Science, Rehovot, Israel

Received: April 25, 2005; In Final Form: June 28, 2005

The ^{17}O hyperfine interaction of the water ligands and the V=O oxygen in the vanadyl aquo complex and of the water ligands in the Mn^{2+} aquo complex in a frozen solution were determined by W-band (95 GHz) electron−nuclear double resonance (ENDOR). Orientation selective ENDOR spectra of the vanadyl complex exhibited two distinct signals assigned to the vanadyl oxygen and the water ligands. The assignment of the signals was done based on the orientation of the principal axis system of the hyperfine interaction and through comparison with the hyperfine interaction predicted by DFT calculations. The latter showed good agreement with the experimental values thus providing clear evidence that the vanadyl oxygen is exchangeable. The interaction of the vanadyl oxygen, especially its anisotropic part, was significantly larger than that of the water oxygens due to a relatively large negative spin density on the oxygen p orbitals. The ^{17}O hyperfine interaction of the water ligand in the Mn^{2+} complex was found to be similar to that of the water ligand in the vanadyl complex and was in good agreement with earlier single-crystal data. Here, due to the large thermal polarization, it was also possible to determine the absolute sign of the hyperfine coupling by selecting different EPR transitions.

Introduction

Electron Nuclear Double Resonance (ENDOR) is a well-established tool to reveal the coordination environment of transition metal ions in a variety of systems. When the nuclear spin of interest has $I = {}^1/_2$, such as in the case of ^1H, ^{13}C, ^{15}N, and ^{31}P, the ENDOR spectra of frozen solutions or polycrystalline samples are relatively easy to interpret because they are dominated by only one anisotropic interaction—the hyperfine interaction. Another popular nucleus in ENDOR spectroscopy is ^2H, with $I = 1$, which exhibits a small quadrupolar interaction, the amplitude and direction of which are usually known. In ^{14}N ($I = 1$) the quadrupolar interaction is larger and depends strongly on the chemical environment, nonetheless ENDOR has been used extensively.[1] ENDOR applications of ^{17}O, $I = {}^5/_2$, are less common due to its low natural abundance and rather complicated spectrum. Its relatively large quadrupole interaction leads to significant broadening of the nuclear $|{}^1/_2\rangle \rightarrow |-{}^1/_2\rangle$ transition, and some of the transitions appear at too low frequencies and are difficult to detect at the conventional X-band frequencies. Moreover, the ^{17}O ENDOR signals often overlap with those of protons.[2] This is unfortunate because ^{17}O is an important probe in many systems in biology, catalysis, and material science that involve metal−oxygen coordination. When the couplings are large they can be resolved in the EPR spectrum, but when they are on the order of a few gauss, they are often hard to resolve. X-band electron spin echo envelope modulation (ESEEM) has been rarely used to probe ^{17}O hyperfine couplings,[3] but recently Q-band HYSCORE (hyperfine sublevel correlation spectroscopy) has been shown to be useful in the determination of ^{17}O hyperfine couplings.[4]

EPR and ENDOR of high spin metal ions is a challenge, especially at the conventional X-band frequencies. For instance, Mn^{2+} has an electronic spin $S = {}^5/_2$ and at 9 GHz the ^{17}O Zeeman interaction is small, hence even at low temperatures all the $M_S = \pm{}^5/_2, \pm{}^3/_2, \pm{}^1/_2$ states contribute to the ENDOR spectrum. In the case of $Mn(H_2O)_6{}^{2+}$ some of the ^{17}O ($\nu_I \approx 2.02$ MHz) signals overlap with the ^1H ($\nu_I \approx 14.90$ MHz).[2] One way to resolve these congested spectra has been to compare samples with ^{16}O and ^{17}O. Another solution can be the combination of different types of techniques, such as ESEEM and (hyperfine selective) ENDOR, and numerical calculations to deconvolute the spectra. These solutions were applied to $Mn(H_2O)_6{}^{2+}$ by Tan et al.[2] Single crystal studies can significantly simplify the spectra, but often it is not feasible to crystallize the desired sample.

Some of the problems listed above can be alleviated by performing ^{17}O ENDOR experiments at high fields, and often the Q-band is sufficient. Continuous wave and pulsed Q-band ENDOR has been found effective for detecting ^{17}O hyperfine couplings in biological systems.[5−7] At high fields the width of the nuclear $|{}^1/_2\rangle \rightarrow |-{}^1/_2\rangle$ transition in orientationally disordered samples is primarily determined by the hyperfine anisotropy due to the reduction in the second-order effects of the nuclear quadrupole interaction. Moreover, the Zeeman interaction is much larger, thus separating the oxygen signals from those of the protons. For example, W-band (95 GHz) ^{17}O ENDOR was recently used to investigate the coordination of Gd^{3+} ions ($S = {}^7/_2$) to $H_2{}^{17}O$ ligands in an aquo-complex and in a complex with the MRI contrast agent MS-325 in an ^{17}O enriched frozen water/methanol solution. In both cases the ^{17}O exhibited a rather small hyperfine coupling (1−2 MHz) and the quadrupolar splittings could be resolved.[8] Here we applied W-band ENDOR to metal ion complexes with $H_2{}^{17}O$ in frozen solutions, where the ^{17}O exhibits relatively large couplings. Initially, we characterized the ^{17}O hyperfine couplings of $Mn(H_2O)_6{}^{2+}$, which have already been studied at X-band frequencies, as a model to demonstrate the advantages of high field ENDOR, particularly for the determination of the absolute sign of the hyperfine couplings. Then we proceeded to $VO(H_2O)_5{}^{2+}$, where the ^{17}O signals of

10.1021/jp052132q CCC: $30.25
Published on Web 08/12/2005

the equatorial water ligands and the vanadyl oxygen were resolved and their hyperfine interactions were determined. The assignment was based on the orientation of the hyperfine interaction of the latter with respect to the g-tensor and on DFT calculations.

The chemistry of the VO^{2+} ion is very diverse and has been extensively reviewed.[9,10] It is a d^1 system and thus EPR spectroscopy played a vital role in unraveling the electronic structure of vanadyl species.[9−13] The vanadyl ion VO^{2+}, has the advantage that it can substitute for Mg^{2+}, Ca^{2+}, and Zn^{2+} in biological systems that are EPR silent.[10] Apart from the d^1 electronic configuration, the isotopic purity of the natural occurring ^{51}V and the high nuclear spin ($I = {}^7/_2$) make VO^{2+} a very attractive EPR probe. The Mn^{2+} ion is an important center in enzymes, more in particular due to its binding to oxygen at active sites.[14−16] Mn^{2+} has also been used as an EPR probe, substituting for Mg^{2+}, a common physiological cofactor, for instance in phosphate kinases.[17] Both Mn^{2+} and VO^{2+} often coordinate to water/OH or other oxygen based ligands, therefore, the present work can serve as a reference for future studies of unknown systems involving these metal ions.

Experimental Section

Sample Preparation. $MnCl_2 \cdot 2H_2O$ (Merck) and $VOSO_4$(aq) (Fluka) were dissolved in methanol to obtain concentrations of 4 mM. Small amounts of these solutions were mixed with $H_2{}^{17}O$ (41.6 wt % isotopic purity, Di-Chem Inc.) in a 1:1 ratio, yielding a final metal ion concentration of 2 mM.

Spectroscopic Measurements. W-band pulsed EPR and ENDOR experiments were carried out at 94.9 GHz at ∼5 K ($Mn(H_2O)_6{}^{2+}$) and ∼7.5 K ($VOSO_4$(aq)) on a home-built spectrometer.[18] Field-sweep echo detected (FS-ED) spectra were collected using the two-pulse sequence $\pi/2-\tau-\pi-\tau-$echo) where the echo intensity was recorded as a function of the magnetic field. In this experiment, microwave (MW) pulse lengths (t_{MW}) of 0.04/0.08 μs ($VOSO_4$(aq)) and 0.03/0.06 μs ($Mn(H_2O)_6{}^{2+}$) with $\tau = 0.25$ μs were employed. The ^{17}O ENDOR spectra were recorded using the Davies ENDOR[19] sequence ($\pi-T-\pi/2-\tau-\pi-\tau-$echo with a radio frequency (rf) pulse during time T) with $t_{RF} = 35$ μs and $\tau = 0.35$ μs, using the random acquisition mode.[20] For the VO^{2+} aquo complex, t_{MW} of 0.05 and 0.10 μs and for the Mn^{2+} aquo complex 0.10 and 0.20 μs were used for the $\pi/2$ and π pulses, respectively. The number of accumulations were around 200 for the ^{17}O ENDOR spectra of the VO^{2+} (except the spectrum at 3.481 T) and around 500 for the Mn^{2+} aquo complex and the 3.481 T spectrum of the VO^{2+} complex.

Simulations. ENDOR simulations were carried out using a program based on EasySpin.[21] The ENDOR frequencies of any electron spin, S, coupled to n nuclear spins, each with a nuclear spin I_i, are derived from the following general Hamiltonian.

$$\hat{H} = \frac{\beta}{h}\vec{B}\cdot\mathbf{g}\cdot\hat{S} + \hat{S}\cdot\mathbf{A}\cdot\hat{I} + \hat{S}\cdot\mathbf{D}\cdot\hat{S} + \sum_{i=1}^{n}\left[-\frac{g_{n,i}\beta_n}{h}\vec{B}_0\cdot\hat{I}_i + \hat{S}\cdot\mathbf{A}_i^{\,L}\cdot\hat{I}_i + \hat{I}_i.\mathbf{Q}.\hat{I}_i\right] \quad (1)$$

The first three terms, the electron Zeeman, the central atom hyperfine, and the zero field splitting (ZFS) interactions comprise the major electron spin interactions whereas the last three terms are related to the nuclear ligand interactions. The first corresponds to the nuclear Zeeman interaction, the second to the ligand hyperfine interaction and the last term is due to the quadrupole interaction. Since the experiments were done at a high field, the effect of the ZFS on the nuclear frequencies can be neglected, especially for the relatively small ZFS of the Mn^{2+} aquo complex.[22] It is convenient to express $\vec{B}$, **A**, and **Q** in the principal axis system of the g-tensor (X,Y,Z). **A** and **Q** are characterized by their principal components, (A_{xx}, A_{yy}, A_{zz}) and (Q_{xx}, Q_{yy}, Q_{zz}) (or $A_{||}$ and $A_{\perp}$ for an axially symmetric tensor) and the Euler angles (α, β, γ) and (α', β', γ'), which relate the **A** and **Q** principal axis systems to that of **g**(X,Y,Z). When **g** is axially symmetric there is no dependence on α, which can therefore be set to zero. The anisotropic part of **A** is represented by **T** and the isotropic part by a_{iso}. The first-order expression for the ENDOR frequencies for a weak coupling case, with the quadrupole interaction, is[23]

$$\nu_{ENDOR} = M_S A - \nu_I(^{17}O) + P(2M_I - 1) \quad (2)$$

where $\nu_I = (g_n\beta_n/h)B_0$ is the nuclear Larmor frequency and M_S and M_I are the electron spin and nuclear spin projections, respectively. A and P are the effective hyperfine and quadrupole couplings, which are a function of β, γ and β', γ' and the orientation of $\vec{B}$ with respect to (X,Y,Z), given by θ_0 and ϕ_0. The principal values of **Q** are: $e^2qQ/(h4I(2I-1))$ [$-1+\eta$, $-1-\eta$, 2]. The simulation of the ^{17}O ENDOR spectrum of $Mn(H_2O)_6{}^{2+}$ measured at the field position where the $|-{}^3/_2,M_I\rangle \rightarrow |-{}^1/_2,M_I\rangle$ EPR transitions are the main contributors to the EPR signal, was obtained by taking half of the simulated spectrum for a $S = {}^3/_2$ system, containing the $M_S = -{}^1/_2, -{}^3/_2$ signals.

For electron−nuclear distances, r, greater than 2.5 Å, and for the case when the spin delocalization over the ligand is negligible, $T_{\perp}$ can be described by the point-dipole approximation:

$$T_{\perp} = \frac{\mu_0\rho^{\alpha-\beta}}{4\pi h}\frac{g_e\beta_e g_n\beta_n}{r^3} \quad (3)$$

Here $\rho^{\alpha-\beta}$ is the spin density.

When pulsed EPR experiments are carried out on a sample with an anisotropic EPR powder pattern, only a selected range of θ_0 and ϕ_0 orientations, determined by the field position within the powder pattern, contribute to the echo.[24,25] These selected orientations can be obtained from simulations of the EPR spectrum, taking into account the line width and the MW pulse bandwidth.[26] Such simulations were carried out using the EPR simulation program developed by Frank Neese.[27]

DFT Calculations. The geometries of the complexes studied in this work were optimized with Gaussian 03, using an unrestricted B3LYP functional[28−30] and a 6-31G(d)[31] basis set. For the vanadyl complex we obtained very similar results as received with ADF by Larsen.[32] To be able to compare the results of the DFT calculations for the protons, we used the optimized Cartesian coordinates from this reference. All DFT calculations of hyperfine couplings and g-tensors were carried out with the ORCA program package.[33] An initial convergence was reached with the basis 3-21G[34] for all atoms and the BP86 functional.[28,35] This result was used as an input for the calculations using the hybrid functional B3LYP[28−30] employing the EPR−II[36] basis sets for the oxygens and protons with an appropriate auxiliary basis set. For the metal the accurate triply polarized basis set CP(PPP)[37] was used with an appropriate integration grid. This is an all electron basis set with added flexibility in the core region, which is necessary to describe properties like isotropic hyperfine coupling and field gradient,

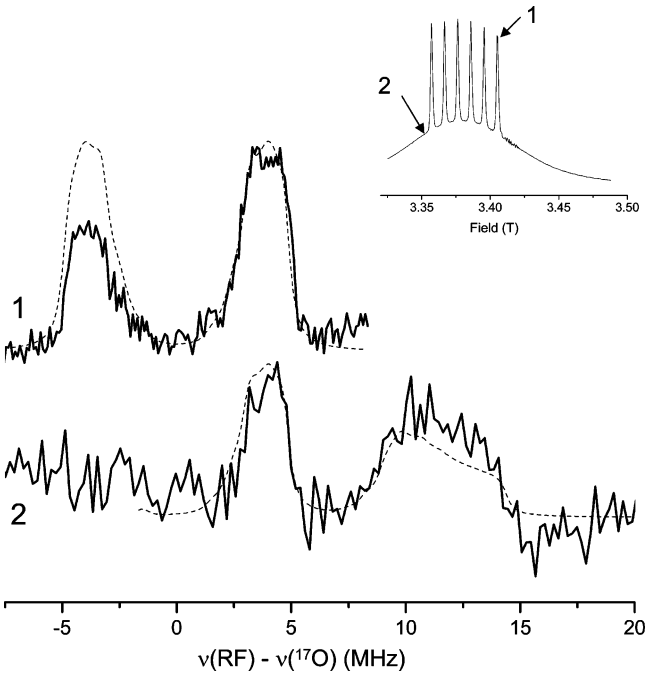

Figure 1. ^{17}O Davies ENDOR spectra of the Mn^{2+} aquo complex at two different field positions, which are indicated on the field sweep echo detected spectrum (inset).

which are influenced by the spin- and charge distribution in the core region. The CP basis is based on the TurboMole DZ basis developed by Ahlrichs and co-workers and obtained from the basis set library under ftp.chemie.uni-karlsruhe.de/pub/basen. For the metal, the polarization sets consisted of 2p functions according to Wachters[38] and a 1f-function taken from the aforementioned Turbomole library. The g-tensors were calculated via the coupled-perturbed SCF equations and the origin was chosen at the center of electronic charge. The parametrization of Koseki was used for the spin−orbit coupling operator.[39]

Results

W-Band ^{17}O Davies ENDOR Measurements. ^{17}O Davies ENDOR measurements were carried out on the Mn^{2+} aquo complex at two different field positions and the results are shown in Figure 1. At the first field position, indicated by number **1** in the FS-ED spectrum (inset of Figure 1), the ENDOR spectrum shows a doublet situated symmetrically around the Larmor frequency of ^{17}O. The lines have a splitting of 8 MHz and are about 2.5 MHz wide (half-height). At this field, 3.41 T, the $|-1/2, 5/2\rangle \rightarrow |1/2, 5/2\rangle$ EPR transition is selected predominantly and the corresponding ENDOR signals show at $\nu_I(^{17}O) \pm A/2$, according to eq 2 (quadrupolar splittings are unresolved). At the low temperatures of these measurements (∼5 K) the thermal polarization is significant, hence the intensity of the $|-3/2, M_I(Mn)\rangle \rightarrow |-1/2, M_I(Mn)\rangle$ transitions are larger than those of the $|3/2, M_I(Mn)\rangle \rightarrow |1/2, M_I(Mn)\rangle$ transitions. Accordingly, the ENDOR spectrum at the field position labeled **2**, 3.35 T, arises mainly from the $|-3/2, M_I(Mn)\rangle \rightarrow |-1/2, M_I(Mn)\rangle$ EPR transitions, resulting in an asymmetric ENDOR spectrum with respect to $\nu_I(^{17}O)$, with the $M_S = -1/2$ manifold line at $-\nu_I(^{17}O) - 1/2A$ and the $M_S = -3/2$ line at $-\nu_I(^{17}O) - 3/2A$ (eq 2).The latter is three times as broad, as expected. From this spectrum the sign of the hyperfine coupling was determined to be negative, according to eq 2 and recalling that $\nu_I(^{17}O)$ is negative. Compared to X-band spectra,[2] the W-band spectra are well resolved and the various spectral components arising from different M_S manifolds are easily detected and assigned. Moreover, the detection of the $M_S = -3/2$ line, for which the hyperfine anisotropy is amplified by a factor of 3, allows to probe small anisotropies, and discern their contribution from that of the quadrupole interaction that does not scale with the M_S value (see eq 2).

The assignment of the +4 MHz component to the $M_S = -1/2$ manifold also accounts for its higher intensity in the 3.41 T spectrum, where the spectrum includes contributions of the $|-3/2, M_I(Mn)\rangle \rightarrow |-1/2, M_I(Mn)\rangle$ transitions at this field. Similarly, the slightly larger intensity of the $|-3/2\rangle$ component in the spectrum recorded at field **2** relative to the simulated spectra probably arises from contributions of the $|-5/2, M_I(Mn)\rangle \rightarrow |-3/2, M_I(Mn)\rangle$ transition. The possibility that the difference in line intensities is a consequence of nuclear polarization, due to an insufficiently long repetition time that prevents complete nuclear spin relaxation, is excluded since it should show a reduced intensity for the $M_S = -1/2$ manifold, rather than the opposite.[40] The spectra were simulated and the calculated traces are shown in Figure 1 as dashed traces and the best fit parameters are listed in Table 1. In the simulations the starting value for the quadrupole coupling parameters were taken from single-crystal measurements,[41] namely $Q_{xx} = Q_{yy} = -0.35$ and $Q_{zz} = 0$ MHz. The relatively low resolution did not allow an accurate determination of the quadrupole parameters.

The anisotropic g of $VO(H_2O)_5^{2+}$ permitted to carry out orientation selective ENDOR measurements. The road map (Figure 2), generated after the simulation of the FS-ED EPR spectrum, links the field position with the selected range of θ_0. Since both the **g** and ^{51}V hyperfine tensors are axially symmetric, the whole 0−180° range of ϕ_0 has to be taken into account at each field position. At field position **1** the selected range of θ_0 is 80−90°, namely the magnetic field is perpendicular to $g_{||}$, which points along the V−O double bond. At this position the ENDOR spectrum, shown in Figure 3 (1), reveals two doublets that are centered around $\nu_I(^{17}O)$, with splittings of 7 and 15 MHz. Variation of the field toward $g_{||}$ results in a decrease in the coupling of the 15 MHz doublet, until it overlaps with the first doublet, which remains invariant. The orientation dependent

TABLE 1: Experimental and DFT Calculated ^{17}O Hyperfine and Quadrupolar Parameters of $VO(H_2O)_5^{2+}$ and $Mn(H_2O)_6^{2+}$

type of oxygen	a_{iso}	A_{xx} (T_{xx})	A_{yy}(T_{yy})	A_{zz}(T_{zz})	α, β, γ	e^2qQ/h	η	α, β, γ	ref
VO^{2+}, eq., exp	7.16	8 (0.84)	6.3 (−0.84)	7.2 (0)	*x*, 0, 0	10.7	0.52	0, 0, 0	this work
VO^{2+}, eq., DFT	6.4	5.7 (−0.7)	6.3 (−0.1)	7.2 (0.8)	*x*, 0, 0	10.7	0.52	0, 0, 0	this work
VO^{2+}, vanadyl, exp	8.4	16 (7.6)	16 (7.6)	−6.9 (−15.3)	0, 0, 0	3.3	0.14	0, 0, 0	this work
VO^{2+}, vanadyl, DFT	8.7	16.5 (7.8)	16.4(7.8)	−6.9 (−15.6)	0, 0, 0	3.3	0.14	0, 0, 0	this work
VO^{2+}, ax., DFT	−1.9	−1.1 (−0.8)	−0.9(−1.1)	−3.8 (1.9)	0, 0, 0	10.7	0.59	90, 90, 0	this work
$Mn(H_2{}^{17}O)_6^{2+}$, exp	−7.5	−6.5 (1.0)	−6.5 (1.0)	−9.6 (−2.0)	0, 0, 0	6.0	1	0, 0, 0	this work
$Mn(H_2{}^{17}O)_6^{2+}$, exp	−7.5	−6.3 (1.2)	−6.3 (1.2)	−10.0 (2.4)		7.0	1		2
$Mn(H_2{}^{17}O)_6^{2+}$, exp	7.4	−6.0 (1.4)	−6.6 (0.8)	−9.6 (−2.2)	0, 0, 0[a]	7.4	1	30, 30, 0	single crystal[41]
$Mn(H_2{}^{17}O)_6^{2+}$, DFT	−11.3	−9.6 (1.7)	−10.8 (0.5)	−13.5 (−2.2)	90, 0, 0	10.5	0.62	0, 90, 0	this work

[a] In the case of Mn^{2+} where g is isotropic, only the relative orientation between the hyperfine and quadrupole interaction should be considered.

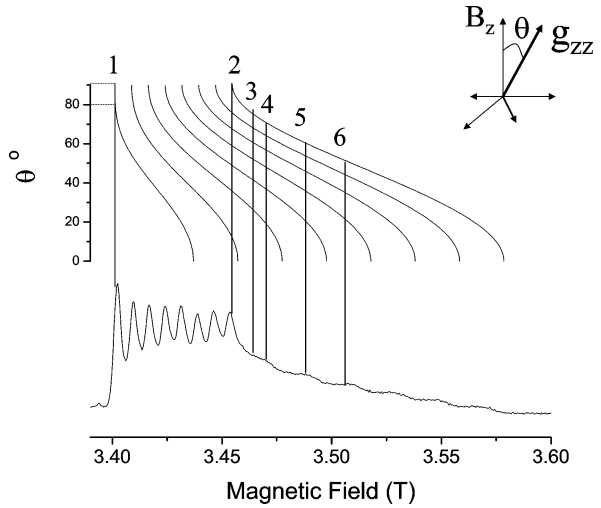

Figure 2. Field sweep echo detected spectrum of the vanadium aquo complex at 94.9 GHz, with the indication of the six different field positions at which ^{17}O Davies ENDOR was carried out and a 'road map' which shows the corresponding θ_0 angles between g_{zz} and the field B_z (inset).

behavior of the large doublet is characteristic of a hyperfine tensor of which the orientation coincides with that of the g-tensor and therefore we assign it to the V═O oxygen. We ruled out the possibility that this doublet is due to an axially ligated water molecule, which should show the same orientation dependence, on the basis of the relatively large coupling. The other doublet is assigned to the equatorial water ligands. As expected, its integrated intensity is significantly larger than that of the vanadyl signals. A resolved signal for an axial water ligand was not detected. Its V−O distance is expected to be larger than for the equatorial ligands. Hence, either its signal overlaps with those of the equatorial ones, within the range closer to $\nu_I(^{17}O)$, or the coupling is too small to be observed by Davies ENDOR.

The spectra at the different field positions were simulated and are shown in Figure 3. The best fit parameters for the vanadyl oxygen and for the equatorial water ligands were obtained after refining the Hamiltonian parameters obtained from the DFT calculations and will be discussed in the next section.

DFT Calculations. To substantiate the assignment of the ^{17}O signals of the $VO(H_2O)_5^{2+}$ complex, which also provides direct experimental evidence for the exchangeable nature of the vanadyl oxygen, DFT calculations were carried out. Similar calculations have been reported earlier for this complex where the hyperfine values of the protons were analyzed and found to be comparable to experimental values.[32] The *g* and ^{51}V hyperfine components obtained using the geometry optimized structure of $VO(H_2O)_5^{2+}$ are given in Table 2 and are compared to our experimental values and to other literature reported experimental values. In Table 2 we also list other DFT calculated values obtained with ADF[42] and ORCA.[43] In general, the calculated *g* values show a reasonable agreement with the experiment, albeit not as close as the ones obtained by Carl et al.[42] The agreement in the case of the ^{51}V hyperfine parameters, however, is better. The latter are in concordance with the results obtained by Neese, using a B3LYP or BP functional.[43] The good agreement for **g** and **A**(^{51}V) serves as an indication that the optimized structure is a good model of the real structure.

The DFT results for the oxygen hyperfine couplings of $VO(H_2O)_5^{2+}$ are listed in Table 1. We have simulated the experimental spectra using the DFT values and the results are presented in Figure 3a. The dashed line is the result for the axial water ligand, not observed (or resolved) in the experiments. In the case of the equatorial water ligands, the simulations were done for only one oxygen out of the four equatorial ligands. A satisfactory fit was obtained, but increasing the A_{xx} value improved the fit, as shown in Figure 3b. and the new value is listed in Table 1 as "exp" . The sign of the equatorial oxygens' hyperfine coupling has not been determined experimentally because the relatively low signal-to-noise ratio made variable mixing time ENDOR measurements, used to determine the sign, difficult.[40,44] The DFT results gave different α angles of the **A** tensor for the different equatorial water ligands, changing this number did not make a significant difference in the simulations due to the axial symmetry of the g-tensor; hence, we represent

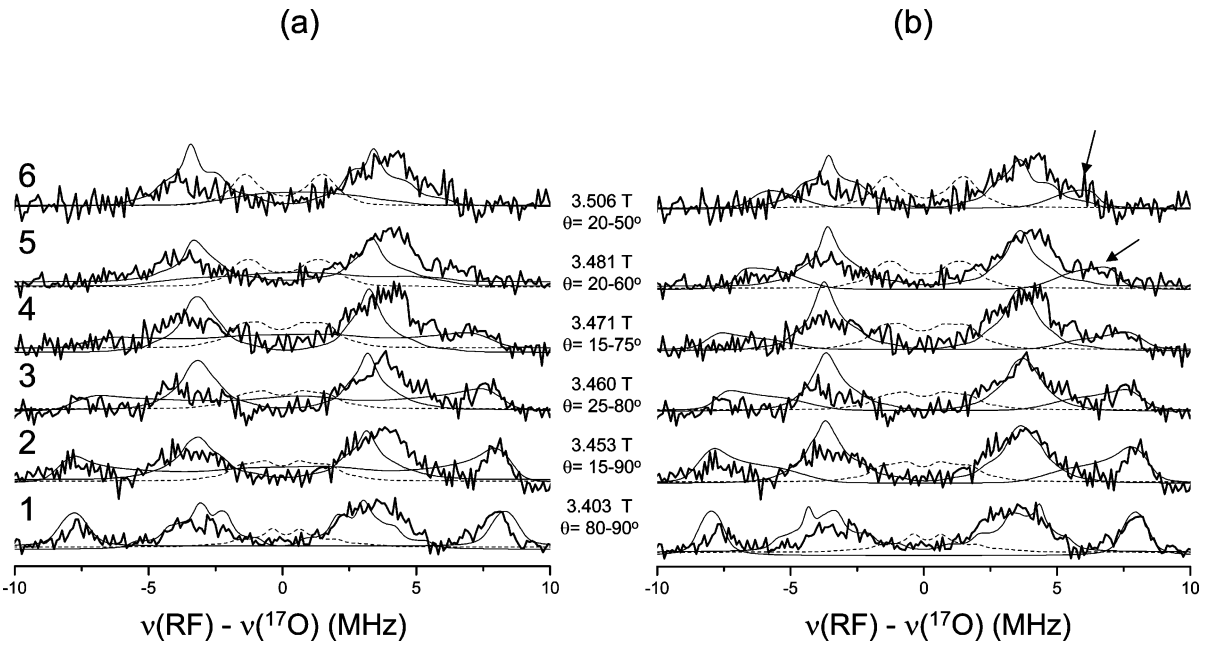

Figure 3. ^{17}O Davies ENDOR of the vanadium aquo complex at different field positions (thick line), the fields and corresponding angles obtained from the road map in Figure 2 are noted next to each spectrum. Also depicted are the simulations of the ^{17}O ENDOR spectra of the individual types of oxygen nuclei (dashed line corresponds to the axial water ligand) of the vanadium aquo complex at different field positions (a) according to the parameters obtained from DFT and (b) with parameters listed in Table 1 as "exp". The arrow marks a shoulder at ∼7 MHz (see text).

TABLE 2: Experimental and Calculated *g* and ^{51}V Hyperfine Principal of Values $VO(H_2O)_5^{2+}$

	g_{xx}	g_{yy}	g_{zz}	ref	A_{xx}, MHz	A_{yy}, MHz	A_{zz}, MHz	ref
exp	1.978	1.978	1.939	this work				this work
exp	1.978	1.978	1.933	61	−212	−212	−547	60
exp	1.982	1.982	1.936	62	−210	−210	−534	62
DFT	1.9852	1.9852	1.9495	this work	−190	−190	−500	this work
DFT	1.986	1.986	1.930	42	148	148	408	42
DFT					−180	−171	−496	B3LYP[43]
DFT					−166	−155	−465	BP[43]

this value with "x" . This justifies the inclusion of only one equatorial oxygen in the simulations. The intensities of the simulated traces shown in Figure 3 were scaled to fit the experimental results.

The DFT calculated hyperfine interaction of the vanadyl oxygen shows that both isotropic and anisotropic parts are indeed significantly larger than those of the water ligands, thus confirming our assignment. Simulations using these values produced a rather satisfactory fit presented in Figure 3a. The parameters were further adjusted to improve the fit resulting in a small decrease in A_{xx} and A_{yy} as shown in Figure 3b and Table 1. The spectra recorded at field positions **5** and **6** exhibit a shoulder at ∼7 MHz, marked with arrows in Figure 3b. If this shoulder arises from the vanadyl signal, reproducing it requires a major change in the DFT A_{zz} value, from −6.9 MHz to 8 MHz. Such a large discrepancy, that involves also a sign change is unlikely considering the good agreement with the DFT predictions for A_{xx} and A_{yy}, the S/N limitations and the overlapping signals of the equatorial ^{17}O. Therefore, we adopt the DFT A_{zz} value and the final parameters are listed in Table 1 as "exp" . We note, however, that without the DFT insight the A_{zz} value of 8 MHz would have been considered as highly likely, thus clearly demonstrating the power of DFT in the spectral analysis. In all the aforementioned best fit simulations the ^{17}O quadrupole tensors of the water ligand and the vanadyl oxygen were taken from the DFT calculations. The low resolution prevented an accurate evaluation of this parameter.

The DFT calculated ^{17}O a_{iso} of the axial water ligand is significantly smaller than that of the equatorial ligand and the vanadyl oxygen as listed in Table 1. These results are also introduced in the simulations shown in Figure 3 (dashed lines). As expected the doublet of the axial ligand is situated closer to the $\nu_I(^{17}O)$ and it is not observed in the Davies ENDOR spectrum. As an additional test, the hyperfine values for the protons were calculated by DFT as well and the values obtained were comparable to the values calculated and discussed by Larsen.[32]

While the DFT calculations predicted the spin Hamiltonian parameters for the vanadyl aquo-complex rather well, the results for the Mn^{2+} complex were not as satisfying. For the *g* values an isotropic value of 2.002 was obtained, which is reasonable but the ^{55}Mn isotropic hyperfine value $a_{iso} = -164$ MHz is too far from the experimental value, −245 MHz[45]. This large deviation has been noted earlier by Neese.[43] The sign of the ^{17}O a_{iso}, which was determined experimentally, is well reproduced. This is consistent with our earlier observation from systematic DFT studies of a variety of hyperfine couplings in copper(II) histidine complexes, which shows that DFT predicts the sign of the interaction very well.[46] The magnitude of the isotropic coupling, however, is overestimated by 50%, while the anisotropic part, shows a better agreement in terms of absolute values of A_{zz}, but substantial deviation from axiality was found.

Discussion

^{17}O CW ENDOR measurements have been performed at Q-band at a temperature of 4.2 K on single crystals of magnesium oxide enriched in ^{17}O and containing Mn^{2+} and the hyperfine parameters for the oxygen ligated to the Mn^{2+} were $a_{iso} = -7.5$ MHz and $T_\perp = -1.015$ MHz.[47,48] A single-crystal ENDOR study of $H_2{}^{17}O$ ligated to Mn^{2+} doped into $[LaMg(NO_2)_{12}\cdot 24(H_2O)]$ reported $a_{iso} = -6.4$ and $T_\perp = -1$ MHz.[41] Both these sets of values and their sign are close to those determined in this work for a frozen solution of $Mn(H_2{}^{17}O)_6^{2+}$ (see Table 1). Our values are also similar to those reported by Tan et al.[2] for the aquo complex measured at X-band frequencies.

Similar literature values for single-crystal measurements of the vanadyl aquo complex are not available, but in this case the ^{17}O hyperfine was evaluated by NMR. In the 1960s, it was extensively demonstrated that ^{17}O NMR is suitable for studying metal ion aquo complexes.[49−54] The technique proved to be particularly interesting to examine the exchange rate of water molecules in and out of the hydration sphere of the metal ion. Because of the hyperfine interactions between the paramagnetic ions and the ^{17}O of the water molecules, the transverse NMR relaxation time T_2 of the oxygens decreases considerably.[55] The exchange of ^{17}O in and out of the coordination sphere of the metal ion in dilute aqueous solutions was monitored by the change in the NMR line width of the ^{17}O of the bulk water.[55,56] VO^{2+} has been subjected to this type of study and experimental proof was found by examining chemical shifts of ^{17}O in Dy^{3+} solutions with different amounts of $VOSO_4$[54] for four equatorial water ligands and one, rapidly exchanging, axial ligand. Similar studies were done on vanadyl perchlorate[55] and on vanadyl complexes with chelating ligands.[56] From the transverse nuclear relaxation time of ^{17}O in aqueous vanadyl perchlorate solutions, Wütrich and Connick calculated an ^{17}O hyperfine coupling constant of 3.8 MHz for the equatorial water molecules.[55] With a calculation based on the changes in chemical shift, Reuben and Fiat found the ^{17}O hyperfine coupling of the water ligands in the $VOSO_4$ in an acidified aqueous complex to be 4.4 ± 1.5 MHz, with a positive sign, in contrast to most transition metal−water complexes.[57] The a_{iso} value for the water ligands found in this work, 6.4 MHz, is larger than these reported values. While we did not determine the sign of the a_{iso} experimentally, the DFT calculations, predict it to be positive. This is in agreement with Reuben and Fiat, who pointed out that the only unpaired electron is situated in a b_2 orbital; hence, π bonding is the major pathway of spin-polarization in this complex, resulting in a positive hyperfine coupling.[57] For other metal−aquo complexes, such as those of Ni^{2+}[53] and Cu^{2+},[58] negative hyperfine couplings were measured, suggesting that σ bonding is important in those complexes. The spin densities obtained from the DFT calculations are listed in Table 3. Although for the equatorial water oxygens it is small, the spin density in the p orbitals is significant enough to introduce a considerable deviation from axial symmetry, expected from a dipolar interaction.

TABLE 3: Spin Densities of the Different Complexes Obtained from the DFT Calculations

complex	orbital	DFT (Loewdin)	DFT (Mulliken)
$VO(H_2{}^{17}O)_5{}^{2+}$, ρ(O)	total s	−0.00103	−0.0033
	total p	−0.00329	−0.0087
	total d	0.0007	0.0004
$V^{17}O(H_2O)_5{}^{2+}$, ρ(O)	total s	−0.0012	−0.0024
	p_x, p_y, p_z	−0.090, −0.090, −0.052	−0.084, −0.084, −0.046
	total d	0.0013	0.0008
$V^{17}O(H_2O)_5{}^{2+}$, ρ(V)	d_{xy}, d_{xz}, d_{yz}	0.98, 0.084, 0.084	0.98, 0.088, 0.088
	d_{z^2},$d_{x^2-y^2}$	0.051, 0.010	0.056, 0.011
$Mn(H_2{}^{17}O)_6{}^{2+}$, ρ(O)	total s	0.0067	0.0003
	total p	0.0162	0.0077
	total d	0.0009	0.0004

The VO^{2+} entity is very stable in aqueous solution and therefore the exchange of the oxygen of VO^{2+} is expected to be rather slow,[9] indeed, it is so slow that it cannot be observed by ^{17}O NMR relaxation measurements.[55,56] Therefore, to our knowledge, no NMR data has been presented for the vanadyl oxygen. However, static methods employing ^{18}O have been successful to prove the vanadyl exchange and to determine its rate.[59] Johnson and Murmann also suggested a mechanism for the vanadyl−oxygen exchange, in which an equatorial water is converted to a vanadyl−oxygen by proton transfer to the original vanadyl oxygen, the reaction is base-catalyzed.[59] These studies, combined with the DFT calculations and the orientation behavior of the ENDOR signal support our assignment of the large splitting doublet to the vanadyl oxygen. The axial character of the vanadyl ^{17}O is well reproduced by the DFT calculations and the experimental and calculated hyperfine parameters are very close. While the a_{iso} value of the vanadyl oxygen is not much larger than that of the water ligands, the anisotropic part is considerably larger and it cannot be accounted for just by the shorter V−O distance. The difference arises from the large spin density on the p orbitals: p_x and p_y have 8−9% negative spin density and p_z about 5% (see Table 3). The origin of these large spin densities is spin polarization through overlap with the vanadium d_{xz} and d_{yz} orbitals, forming the π bond, and with the d_{z^2} orbital (σ bond), which contain 8−9% and 5% positive spin densities, respectively.

The exchange of the Mo═O oxygen with ^{17}O in the protein sulfite oxidase has been recently reported. There, Ka-band HYSCORE was used to determine the ^{17}O interactions. Measurements were reported for a single field only and from the splitting and spread of the cross-peaks, the principal components of A were estimated to be 4.3, 5.3, and 4.8 MHz.[4] These are significantly smaller than the values we obtained for the vanadyl ^{17}O and it could be a consequence of the longer Mo═O bond.

Finally, we note that DFT calculations were found to predict all EPR parameters of the vanadyl aquo complex rather well, from the major electron spin interaction to the ligand hyperfine. This is in contrast to the Cu(II) complexes with histidine.[46] Also the results for the quadrupole tensor seem reasonable. Although the resolution was not enough to validate small changes experimentally, they agree with the line width observed. The quadrupole interaction of the equatorial water ligands in the vanadyl complex was found to be significantly larger than that of the V═O oxygen.

Conclusions

It was demonstrated that pulsed ^{17}O ENDOR measurements at W-band yield resolved spectra that can be analyzed to produce the hyperfine tensor. In the case of the $VO(H_2{}^{17}O)_5{}^{2+}$ complex both the magnitude and orientation of the interaction were determined for both the water and vanadyl oxygen. DFT calculations of the hyperfine tensors showed a very good agreement with the experimental values, which were also used to substantiate the signal assignments and thereby confirm the exchangeable character of the V═O oxygen. For the $Mn(H_2{}^{17}O)_6{}^{2+}$, which has a high electron spin, it was possible to determine the absolute sign of the ^{17}O hyperfine couplings. The isotropic and anisotropic hyperfine couplings in the frozen solution were found to be close to values reported earlier for single crystals by X-band ENDOR. The DFT results, however, were only consistent in predicting the signal of the hyperfine interaction but significant deviations were observed for the absolute values.

Acknowledgment. This work was supported by the Binational USA−Israel Science Foundation (BSF) (Grant 2002175) and the German−Israel Foundation for Scientific Research. We thank Carlos Calle y Richter for his help with the DFT calculations, Frank Neese for providing us with the ORCA program and for his help. Finally, we thank A. Raitsimring and A. V. Astashkin for most stimulating discussions.

References and Notes

(1) Goslar, J.; Piekara-Sady, L.; Kispert, L. D. Chapter 6, *Handbook of Electron Spin Resonance, Data Sources, Computer Technology, relaxation, and ENDOR*; Poole, C. P., Jr., Farach, H. A., Eds.; American Institute of Physics Press: St. Louis, MO, 1994.

(2) Tan, X.; Bernardo, M.; Thomann, H.; Scholes, C. P. *J. Chem. Phys.* **1995**, *102*, 2675−2690.

(3) Thomann, H.; Bernardo, M.; Kroneck, P. M. H.; Ullrich, V.; Goldfarb, D. *J. Am. Chem. Soc.* **1995**, *117*, 8243.

(4) Astashkin, A. V.; Feng, C.; Raitsimring, A. M.; Enemark, J. H. *J. Am. Chem. Soc.* **2005**, *127*, 502.

(5) Burdi, D.; Willems, J.-P.; Riggs-Gelasco, P.; Antholine, W. E.; Stubbe, J.; Hoffman, B. M. *J. Am. Chem. Soc.* **1998**, *120*, 12910.

(6) Telser, J.; Emptage, M. H.; Merkle, H.; Kennedy, M. C.; Beinert, H.; Hoffman, B. M. *J. Biol. Chem.* **1986**, *261*, 4840.

(7) Werst, M. M.; Kennedy, M. C.; Beinert, H.; Hoffman, B. M. *Biochemistry* **1990**, *29*, 10526.

(8) Raitsimring, A. M.; Astashkin, A. V.; Baute, D.; Goldfarb, D.; Caravan, P. *J. Phys. Chem. A* **2004**, *108*, 7318.

(9) Selbin, J. *Chem. Rev.* **1965**, *65*, 153.

(10) Smith, T. S., II; LoBrutto, R.; Pecoraro, V. L. *Coord. Chem. Rev.* **2002**, *228*, 1−18.

(11) Eaton, S. S.; Eaton, G. R. In *Vanadium in Biological Systems*; Chasteen, N. D., Ed.; Kluwer: Boston, MA, 1990; p 199.

(12) Makinen, M. W.; Mustafi, D. *Metal Ions in Biological Systems*; Sigel, H., Sigel, A., Eds.; Marcel Dekker: New York, 1995; p 89.

(13) Chasteen, N. D. In *Methods in Enzymology*; Riordan, J. F., Vallee, B. L., Eds.; Academic Press New York, 1993; Vol. 227 (8), p 232.

(14) Reed, G. H.; Markham, G. D. *Biol. Magn. Res.* **1984**, *6*, 73.

(15) Yocum, C. F.; Pecoraro, V. L. *Curr. Opin. Chem. Biol.* **1999**, *3*, 182.

(16) Horsburgh, M. J.; Wharton, S. J.; Karavolos, M.; Foster, S. J. *Trends Microbiol.* **2002**, *10*, 496.

(17) Smithers, G. W.; Sammons, R. D.; Goodhart, P. J.; LoBrutto, R.; Reed, G. H. *Biochemistry* **1989**, *28*, 1597.

(18) Gromov, I.; Krymov, V.; Manikandan, P.; Arieli, D.; Goldfarb, D. *J. Magn. Reson.* **1999**, *139*, 8−17.

(19) Davies, E. R. *Phys. Lett. A* **1974**, *47*, 1.

(20) Epel, B.; Arieli, D.; Baute, D.; Goldfarb, D. *J. Magn. Reson.* **2003**, *164*, 78.
(21) Stoll, S. Spectral Simulations in Solid-State EPR, Ph.D. Thesis, ETH Zürich, 2003; http://www.esr.ethz.ch/EasySpin/.
(22) Vardi, R.; Bernardo, M.; Thomman, H.; Strohmaier, K. G.; Vaughan, D. E. W.; Goldfarb, D. *J. Magn. Reson.* **1997**, *126*, 229.
(23) Piekara-Sady, L.; Kispert, L. D. Chapter 5, *Handbook of Electron Spin Resonance, Data Sources, Computer Technology, relaxation, and ENDOR.* Poole, C. P., Jr., Farach, H. A., Eds.; American Institute of Physics Press: St. Louis, MO, 1994.
(24) Rist, G. H.; Hyde, J. S. *J. Chem. Phys.* **1970**, *52*, 4633.
(25) Hurst, G. C.; Henderson, T. A.; Kreilick, R. W. *J. Am. Chem. Soc.* **1985**, *107*, 7299.
(26) Goldfarb, D.; Fauth, J. M.; Tor, Y.; Shanzer, A. *J. Am. Chem. Soc.* **1991**, *113*, 1941.
(27) Neese, F. Electronic Structure and Spectroscopy of Novel Copper Chromophores in Biology. Ph.D. Thesis, University of Konstanz, 1997.
(28) Becke, A. D. *Phys. Rev. A* **1988**, *38*, 3098.
(29) Lee, C.; Yang, W.; Parr, R. G. *Phys. Rev. B* **1988**, *37*, 785.
(30) Becke, A. D. *J. Chem. Phys.* **1993**, *98*, 1372; *98*, 5648.
(31) Ditchfield, R.; Hehre, W. J.; Pople, J. A. *J. Chem. Phys.* **1971** *54*, 724. Hehre, W. J.; Ditchfield, R.; Pople, J. A. *J. Chem. Phys.* **1972**, *56*, 2257. Rassolov, V. A.; Pople, J. A.; Ratner, M. A.; Windus, T. L. *J. Chem. Phys.* **1998**, *109*, 1223. Hariharan, P. C.; Pople, J. A. *Theor. Chim. Acta* **1973**, *28*, 213.
(32) Larsen, S. C. *J. Phys. Chem. A* **2001**, *105*, 8333.
(33) Neese, F. ORCA—an ab initio, Density Functional and Semiempirical Program Package, version 2.4—Revision 13; Max Planck Institute for Bioinorganic Chemistry: Muelheim/Ruhr, Germany, August 2004.
(34) Binkley, J. S.; Pople, J. A.; Hehre, W. J. *J. Am. Chem. Soc.* **1980**, *102*, 939. Dobbs, K. D.; Hehre, W. J. J. *Comput. Chem.* **1987**, *8*, 861.
(35) Perdew, J. P. *Phys. Rev. B* **1986**, *33*, 8822.
(36) Barone, V. *Recent Advances in Density Functional Methods, Part I*; Chong, D. P., Ed.; World Scientific: Singapore, 1996.
(37) Neese, F. *Inorg. Chim. Acta* **2002**, *337C*, 181.
(38) Wachters, J. *Chem. Phys.* **1970**, *52*, 1033.
(39) Koseki, S.; Gordon, M. S.; Schmidt, M. W.; Matsunaga, N. *J. Phys. Chem.* **1995**, *99*, 12764. Koseki, S.; Schmidt, M. W.; Gordon, M. S. *J. Phys. Chem.* **1992**, *96*, 10768; *J. Phys. Chem. A* **1998**, *102*, 10430.
(40) Epel, B.; Pöppl, A.; Manikandan, P.; Vega, S.; Goldfarb, D. *J. Magn. Reson.* **2001**, *148*, 388.
(41) Glotfelty, H. W. Ph.D. Thesis, University of Kansas, 1978.
(42) Carl, P. J.; Isley, S. L.; Larsen, S. C. *J. Phys. Chem. A.* **2001**, *105*, 4563.
(43) Neese, F. *J. Chem. Phys.* **2003**, *118*, 3939.
(44) Bennebroek, M. T.; Schmidt, J. *J. Magn. Reson.* **1997**, *128*, 199.
(45) Upreti, G. C. *J. Magn. Reson.* **1974**, *13*, 336.
(46) Baute, D.; Arieli, D.; Neese, F.; Zimmermann, H.; Weckhuysen, B. M.; Goldfarb, D. *J. Am. Chem. Soc.* **2004**, *126*, 11733.
(47) Freund, P.; Hahn, B. F.; Owen, J. *J. Phys. C: Solid State Phys.* **1971**, *4*, L296.
(48) Freund, P.; Owen, J.; Hahn, B. F. *J. Phys. C: Solid State Phys.* **1973**, *6*, L139.
(49) Jackson, J. A.; Lemons, J. F.; Taube, H. *J. Chem. Phys.* **1960**, *32*, 553.
(50) Swift, T. J.; Connick, R. E. *J. Chem. Phys.* **1962**, *37*, 307.
(51) Connick, R. E.; Fiat, D. *J. Chem. Phys.* **1963**, *39*, 1349.
(52) Alei, M.; Jackson, J. A. *J. Chem. Phys.* **1964** , *41*, 3402.
(53) Connick, R. E.; Fiat, D. *J. Chem. Phys.* **1966**, *44*, 4103.
(54) Reuben, J.; Fiat, D. *Inorg. Chem.* **1967**, *6*, 579—583.
(55) Wütrich, K; Connick, R. E. *Inorg. Chem.* **1967**, *6*, 583.
(56) Wütrich, K; Connick, R. E. *Inorg. Chem.* **1968**, *7*, 1377.
(57) Reuben, J.; Fiat, D. *Inorg. Chem.* **1969**, *8*, 1821.
(58) Lewis, W. B.; Alei, M., Jr.; Morgan, L. O. *J. Chem. Phys.* **1966**, *44*, 2409.
(59) Johnson, M. D.; Murmann, R. K. *Inorg. Chem.* **1983**, *22*, 1068.
(60) Atherton, N. M.; Shackleton, J. F. *Mol. Phys.* **1980**, *39*, 1471.
(61) Chasteen, N. D. *Biological Magnetic Resonance*; Berliner, L. J., Reuben, J., Eds.; Plenum Press: New York, 1981; Vol. 3, pp 53—119.
(62) Martini, G.; Ottaviani, M. F.; Seravalli, G. L. *J. Phys. Chem.* **1975**, *79*, 1716.